Petroleum Science 23 (2026) 1250–1260

Contents lists available at ScienceDirect

Petroleum Science

journal homepage: www.keaipublishing.com/en/journals/petroleum-science

Original Paper

An improved pulsed neutron method for gas reservoirs identification in the complex buried hill formation of the Bohai Sea

Zhen-Yang Li [a], Jie Shang [b], Jia-Wei Zhang [b], Qiong Zhang [a,*], Quan-Ying Zhang [c]

[a] Department of Control Science and Engineering, School of Automation Engineering, University of Electronic Science and Technology of China, Chengdu, 611731, Sichuan, China
[b] China Oilfield Services Limited, Sanhe, 065201, Hebei, China
[c] College of Geophysics and Petroleum Resources, Yangtze University, Wuhan, 430100, Hubei, China

ARTICLE INFO

Article history:
Received 21 June 2025
Received in revised form
25 November 2025
Accepted 7 January 2026
Available online 13 January 2026

Edited by Meng-Jiao Zhou

Keywords:
The Bohai Sea buried hill
Gas reservoirs identification
The fast neutron elastic scattering cross–section
Lithological profile

ABSTRACT

Recent discoveries revealing the substantial production potential of buried hill reservoirs have spurred significant research interest in their exploration. Pulse neutron logging offers significant advantages for evaluating conventional gas reservoirs. The fast neutron elastic scattering cross–section (FNXS) method combines gamma count rates from detectors at varying distances to effectively identify gas reservoirs. However, the complex lithology and low effective porosity of the Bohai Sea buried hill reservoirs–composed of quartz, feldspar, biotite, calcite, dolomite, and illite–result in significantly reduced accuracy of FNXS–based gas identification. The FNXS equation for a single lithology cannot accurately reflect the comprehensive FNXS of the formation, making it ineffective in indicating gas reservoirs responses.

Therefore, this paper employs the logged wells in the Bohai Sea buried hill as representative study cases. Based on geological information and gamma counts from a pulsed neutron tool, an improved FNXS–based method for gas reservoirs identification in the complex formation is developed through theoretical analysis and numerical simulations. Firstly, key mineral information provided by the XRF–calibrated lithology profile is used to construct an inversion model database for single–mineral FNXS. Based on the mineral content of different intervals, the FNXS inversion formula is adaptively constructed from the database to accurately calculate the comprehensive formation FNXS ($FNXS_{lith}$). Simulation results verified that the error between $FNXS_{lith}$ and the theoretical value is within 1%, which is significantly lower than that of the conventional method. Secondly, to eliminate the interference of matrix FNXS variations on gas reservoirs identification, the comprehensive FNXS of the water–saturated formation ($FNXS^{w}_{sum}$) is calculated using the effective porosity curve. Gas reservoirs are dynamically identified by depth-dependent comparison between these two curves.

The method is validated using data from two wells (X and Y) in the Bohai Sea buried hill, which contain both carbonate formation from the Paleozoic and granitic gneiss formation from the Archean. The proposed dynamic gas reservoirs identification method can effectively indicate gas reservoirs. The identification results are consistent with gas logging curves and DST test results, verifying the reliability of the method.

1. Introduction

Pulse neutron logging, as a widely used method in nuclear geophysical exploration, has certain advantages in conventional gas reservoirs evaluation due to its minimal influence by pore structure, sensitivity to low porosity and formation fluids, and ability to measure a variety of formation parameters(Al-Qasim et al., 2019; Carpenter, 2018; Liu et al., 2018; Zett et al., 2012). In 2007,

* Corresponding author.
E-mail address: zhanqio@uestc.edu.cn (Q. Zhang).
Peer review under the responsibility of China University of Petroleum (Beijing).

https://doi.org/10.1016/j.petsci.2026.01.011

Badruzzaman et al. (2007) used PNC technology to calculate formation Sigma, and combined inelastic gamma counting and gamma count ratios to determine density and evaluate gas reservoirs. In 2006, Trcka et al. (2006) proposed using the ratio of inelastic gamma counts from short and long detectors, along with the capture gamma count ratio, for gas reservoirs identification. They established response maps of the count ratios under different formation conditions through numerical simulations, and combined these with well log data to evaluate gas reservoirs. Scholars have utilized logging tools with ultra–long source–to–detector spacing for the quantitative determination of gas saturation (Guo et al., 2010a, 2010b; Kim et al., 2017; Kwong et al., 2013). In 2016, Zhou et al. (2016) introduced a new formation parameter, the 14 MeV fast neutron elastic scattering cross–section (FNXS), for identifying and quantitatively evaluating gas reservoirs. The FNXS of gas differs significantly from that of rock matrix, water, oil, and other materials. This cross–section is calculated using the inelastic gamma counts from the long detector of a new pulsed neutron logging instrument. The FNXS method inverts the fast neutron elastic scattering cross section of formation based on inelastic gamma counts. By utilizing the extremely low cross section characteristic of gas, it enables effective identification of gas reservoirs while mitigating the influence of the gas excavation effect. This method has attracted considerable attention in low–porosity and geologically complex reservoirs. In 2017, Rose et al. (2017) used a new pulsed–neutron tool to simultaneously measure Sigma, porosity, FNXS, and elemental concentrations, and applied a weighted least–squares linear volumetric model to determine multiphase fluid saturations. In 2019, Li et al. (2019) identified gas or CO_2–reservoirs intervals by combining FNXS, neutron porosity, and density through curve overlap, parameter cross–plots, and a linear volumetric model, achieving good performance in low–porosity Paleozoic reservoirs in the Ordos Basin.

These formations experienced long–term uplift, weathering and erosion before being buried beneath later sediments, forming the Bohai Sea buried hill reservoirs. Recent breakthrough discoveries in the buried hill domain have demonstrated its immense exploration potential (Hu et al., 2017; Li et al., 2021; Wang et al., 2019; Hou et al., 2019). However, due to significant differences in lithology and petrophysical properties between the Bohai Sea buried hill reservoirs and conventional reservoirs. As shown in Fig. 1, the lithology of these reservoirs is complex and variable, consisting of Paleozoic carbonate rocks and Archean granite gneiss, with diverse mineral types including quartz, feldspar, biotite, calcite, dolomite, illite, kaolinite, and chlorite. Although the FNXS is highly sensitive to gas, often showing a sharp decline in gas reservoirs, variations in the FNXS response can also arise from differences in the matrix minerals of the formation itself. Meanwhile, low primary porosity reduces the contribution of pore fluids to the logging tool response, which may obscure the presence of certain gas reservoirs. Consequently, the traditional FNXS method faces limitations in accurately identify and evaluate gas reservoirs under such conditions.

Fig. 1. The rock samples from the Bohai Sea buried hill formation.

In this study, an improved FNXS–based method for gas reservoirs identification in the complex buried hill formations of the Bohai Sea is proposed. This method utilizes lithological information provided by the lithology profile calibrated through X–ray fluorescence (XRF) measurements. On the one hand, the accuracy of integrated formation FNXS calculation is improved by using the key minerals contents provided by the lithology profile to perform a weighted calculation based on the single–mineral FNXS inversion formulas. On the other hand, the accuracy of gas reservoirs identification is enhanced by constructing a dynamic gas reference value–namely, the comprehensive FNXS of the water–saturated formation–to address the interference caused by variations in matrix FNXS. This method is designed to overcome the challenges in gas reservoirs identification caused by lithological heterogeneity.

2. Methodology

As illustrated in Fig. 2, the significant fluctuations in scattering resonance cross-sections observed at low energies—particularly in heavy elements—tend to diminish as neutron energy approaches 14 MeV. At this high-energy threshold, the microscopic cross-sections of various elements converge toward a similar value. Consequently, the elastic scattering cross-section at 14 MeV is employed as a representative parameter for the fast neutron cross-section in the high-energy regime.

The macroscopic scattering cross-section for neutrons in one cubic meter (1 m^3) of any substance can be calculated using the following expression:

$$\Sigma = N_A \cdot \frac{\rho \cdot 10^{-22}}{M} \sum_{i=1}^{m} n_i \cdot \sigma_i \tag{1}$$

where Σ denotes the macroscopic neutron capture cross–section of a substance, m^{-1}; N_A and M represent Avogadro's constant and the molar mass of the molecule, g/mol; ρ is the density of the substance, g/cm^3; m is the number of elemental species constituting the substance; n_i is the quantity of the i–th constituent; σ_i is the microscopic neutron scattering cross–section of the i–th element, in barn.

Utilizing microscopic data sourced from the ENDF/B-VIII.0 database (Chadwick et al., 2006), the elastic and inelastic fast neutron scattering cross-sections for typical reservoir materials were evaluated via Eq. (1). The results indicate a sharp divergence in FNXS between methane and other components (formation matrix, oil, and water). In contrast, the cross-sectional values for the matrix, water, and oil are relatively close. Notably, the methane-matrix contrast is the most significant, whereas the disparity between water and the matrix remains minimal.

Additionally, the direct link between density and the inelastic scattering cross-section implies a mutual cancellation between the generation and attenuation of inelastic gamma rays. As a result, the use of the 14 MeV elastic scattering cross-section as a proxy for gas reservoir evaluation exhibits superior efficacy.

Zhou et al. (2016) demonstrated the use of the pure inelastic gamma count rate from the instrument's long detector as a linear

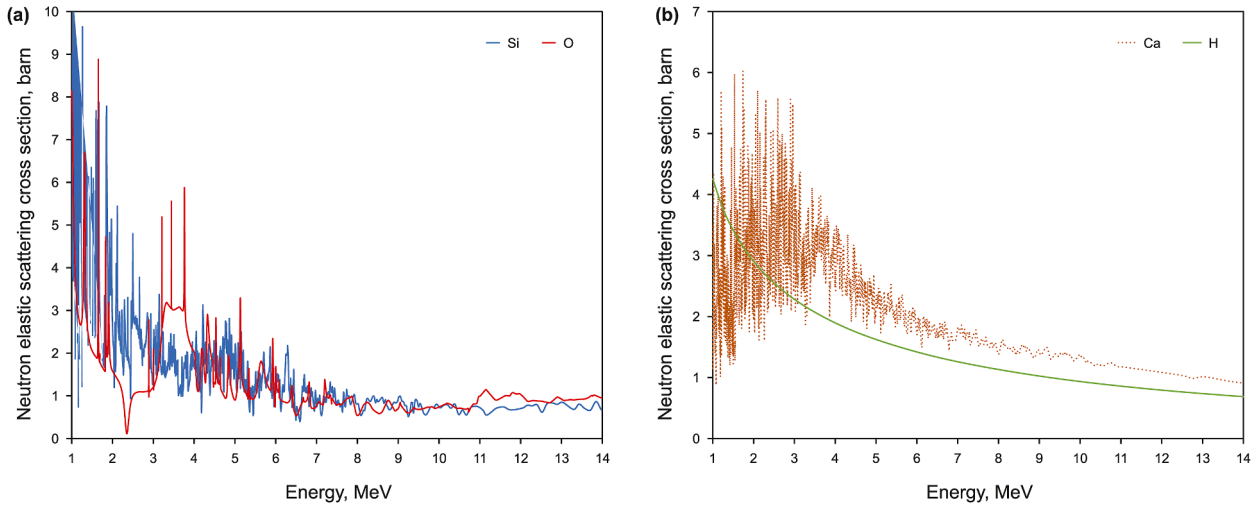

Fig. 2. Neutron elastic scattering cross sections (in barn) for common elements. **(a)** Silicon (Si) and oxygen (O); **(b)** calcium (Ca) and hydrogen (H).

proxy for the fast neutron elastic scattering cross-section of the formation. This relationship is formulated as follows:

$$\mathrm{FNXS} = \frac{1}{a_1 \cdot \log(\mathrm{GRAT}) + a_2} + a_3 \tag{2}$$

where $a_{1,2,3}$ denotes the coefficient, and GRAT represents the inelastic gamma count rate, which has been normalized relative to the output fluctuations of the pulsed neutron source.

Within the framework of neutron–gamma coupling field theory, the inelastic scattering gamma flux is expressed by the following equation (Fan et al., 2024):

$$\varnothing_{\mathrm{in}}(R) = \frac{i\sum_{\mathrm{in}} S_0 \int_0^R \mathrm{e}^{-r/\lambda_s} \mathrm{e}^{-\rho\mu_{\mathrm{m}}(R-r)}\,\mathrm{d}r}{4\pi R^2} = \frac{i\sum_{\mathrm{in}} S_0}{4\pi R^2}\left(\frac{\mathrm{e}^{-R/\lambda_s} - \mathrm{e}^{-\rho\mu_{\mathrm{m}}R}}{\rho\mu_{\mathrm{m}} - 1/\lambda_s}\right) \tag{3}$$

where the parameters are defined as follows: r and R represent the source-to-detector distance and the long-detector spacing, S_0 is the neutron source intensity, λ_s is the mean free path of fast neutrons, $\varnothing_{\mathrm{in}}$ and $\sum_{\mathrm{in}}$ describe the inelastic gamma flux and the scattering cross-section, ρ and μ_{m} refer to the formation volume density and mass attenuation coefficient, i is the inelastic photon yield per neutron collision.

As indicated by Eq. (3), the inherent variability in physical parameters (μ_{m}, ρ) across different reservoirs, coupled with the mineralogical heterogeneity and lithological complexity of the Bohai Sea buried hill formation, suggests that applying Eq. (2) for FNXS estimation in such environments is inherently constrained.

As shown in Fig. 3, four typical mineral assemblages commonly co–existing within the Bohai Sea buried hill formation were selected to analyze how variations in the matrix minerals influence both the matrix and fluid FNXS responses. When the formation porosity is below 10%, the FNXS differences caused by the matrix variations are approximately 25% greater than the FNXS contrast between gas and water. This indicates that, in buried hill reservoirs, the FNXS response used for gas–water identification may be strongly influenced by the matrix mineral variability rather than fluid effects alone. Therefore, lithology correction of the FNXS curve is necessary before applying FNXS for gas reservoirs identification in such complex formation.

As shown in Fig. 4, this study proposes a lithology weighting method for calculating the $\mathrm{FNXS_{lith}}$ to identify gas reservoirs. On

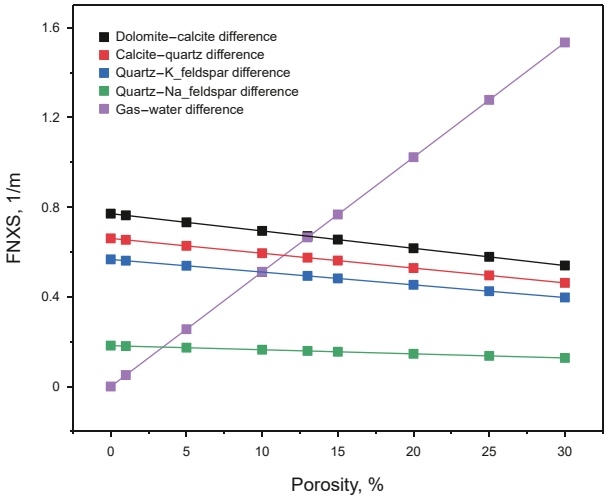

Fig. 3. Effects of matrix variability on gas–water identification using FNXS.

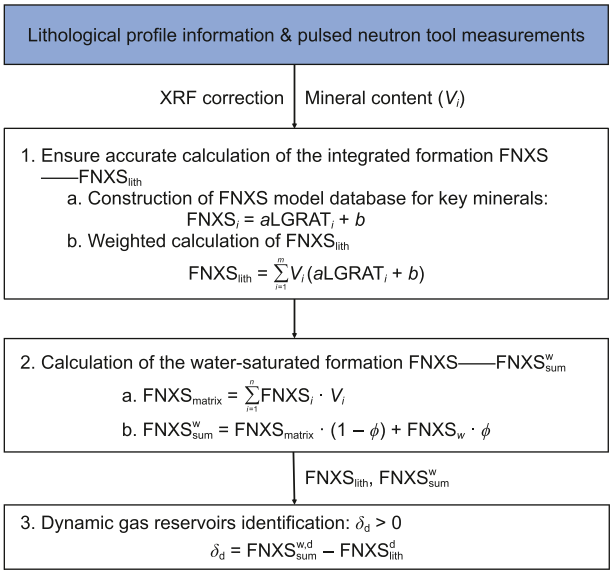

Fig. 4. Method framework of this study.

the one hand, Eq. (2) is suitable for formation with a single lithology. However, due to the diverse mineral compositions in the buried hill formation, the influence of different lithologies must be considered when estimating formation FNXS using the formula fitted from the inelastic gamma counts. Therefore, the lithology profile corrected by XRF provides the contents of key minerals, based on which the FNXS inversion model is constructed for different formation intervals. $FNXS_{lith}$ is then calculated by weighting the inversion equations of individual minerals according to their respective contents. On the other hand, $FNXS_{matrix}$ of the formation is derived using a petrophysical volumetric model, based on either the elemental concentrations provided by XRF or the mineral composition obtained from the lithology profile. Then, in combination with the effective porosity curve, the formation FNXS under full water saturation conditions ($FNXS^{w}_{sum}$) is calculated. Finally, $FNXS^{w}_{sum}$ was used as a reference value of the formation matrix for dynamic calibration of the gas reservoirs.

2.1. Method for calculating $FNXS_{lith}$ based on lithology weighting

To fully eliminate the impact of complex lithology on FNXS calculation, the lithology profile was first calibrated using the elemental contents of the matrix minerals obtained from XRF elemental logging (Kowalska et al., 2020), which provides accurate identification of the key matrix minerals and their contents.

Then, based on the lithology information, the FNXS model database for key minerals in the buried hill formation is constructed using Eq. (2). A Geant4–based numerical model is employed to simulate the FNXS responses of gas–saturated and water–saturated formation, assuming the matrix consists of a single mineral. Inversion formulas for formation FNXS corresponding to each key mineral as the sole matrix were derived and fitted to establish the model database. Eq. (4) presents the inversion formula for the integrated formation FNXS ($FNXS^{i}_{sum}$) when the matrix consists of a specific mineral:

$$FNXS^{i}_{sum} = a \cdot LGRAT_i + b \tag{4}$$

where a is the fitting coefficient, $LGRAT_i$ is the logarithm of the inelastic gamma counts from the long detector, and b is a constant.

The key point lies in the adaptive construction of FNXS inversion models for different intervals in complex reservoirs by applying a weighted approach based on the contents of key formation minerals provided by the lithology profile. The model is defined as shown in Eq. (5).

$$FNXS_{lith} = \sum_{i=1}^{m} V_i \cdot FNXS^{i}_{sum} \tag{5}$$

where m is the number of key mineral types present in the formation, and V_i represents the volume fraction of the i–th mineral.

2.2. Method for calculating $FNXS_w$ based on the petrophysical volumetric model

According to the petrophysics volume model, the integrated FNXS under water–saturated conditions ($FNXS^{w}_{sum}$) of can be represented by the $FNXS_{matrix}$, the FNXS of freshwater ($FNXS_w$), and the porosity($\varnothing$), as expressed by the following Eq. (6):

$$FNXS^{w}_{sum} = FNXS_{matrix} \cdot (1 - \varnothing) + FNXS_w \cdot \varnothing \tag{6}$$

The matrix in the Bohai Sea buried hill formation has a complex rock mineral composition. The FNXS of the matrix is calculated by weighting the FNXS of each mineral. Assuming the formation consists of n minerals, with the volume fraction of each mineral being V_i, the FNXS value of the formation matrix can be expressed as:

$$FNXS_{matrix} = \sum_{i=1}^{n} FNXS_i \cdot V_i \tag{7}$$

The $FNXS_{matrix}$ can be calculated either from the key matrix minerals and their contents provided by the lithology profile calibrated using XRF elemental logging, or directly from the elemental composition of the matrix obtained from XRF measurements (Li et al., 2025).

After determining the matrix minerals, the integrated FNXS of the formation under water–saturated conditions in complex reservoirs can be calculated using Eq. (6) in combination with the effective porosity curve.

2.3. Reservoirs gas content evaluation method

Compared with conventional reservoirs, the matrix FNXS varies significantly across different intervals in buried hill complex reservoirs, making it difficult to use a single reference value for gas reservoirs calibration over the entire well interval. Therefore, this study proposes a dynamic gas reservoirs calibration method:

After the lithology–weighted inversion in Section 2.1 and the petrophysical volumetric calculation in Section 2.2, both $FNXS_{lith}$ and $FNXS^{w}_{sum}$ are corrected for the effects of matrix mineral variations. As a result, their responses are no longer influenced by changes in matrix minerals across different intervals, enabling gas–water discrimination to be driven purely by fluid effects rather than lithological heterogeneity. Therefore, instead of using a single fixed reference value for the entire well interval, this study proposes a dynamic gas reservoirs calibration method based on the depth–dependent comparison between $FNXS_{lith}$ and $FNXS^{w}_{sum}$:

$$\delta_d = FNXS^{w,d}_{sum} - FNXS^{d}_{lith} \tag{8}$$

$FNXS^{w,d}_{sum}$ represents the comprehensive formation FNXS at depth d when the formation is fully saturated with water, and $FNXS^{d}_{lith}$ represents the comprehensive formation FNXS at depth d calculated from the measured gamma information.

At a given depth point d, when $\delta_d > 0$, the formation intergrated FNXS calculated by lithology weighting averaging is less than the intergrated FNXS of the formation fully saturated with water at that depth, the interval is identified as a gas reservoir.

This dynamic gas reservoirs evaluation method effectively addresses the difficulty of identifying gas reservoirs caused by lithological variations in buried hill reservoirs, thereby improving the sensitivity of gas reservoirs recognition.

3. Monte Carlo numerical simulation and discussion

By integrating authentic nuclear reaction cross-section libraries with stochastic mathematical principles, Monte Carlo simulation effectively models the coupled transport of neutrons, photons, and electrons. In this study, we utilized Geant4 to construct a comprehensive tool–borehole–formation model, aiming to assess gas reservoirs via pulsed neutron technology (Velker et al., 2012). Specifically, the transport of fast neutrons and gamma rays was simulated to investigate how environmental variables influence gas identification when using the pulsed neutron cross-section technique. Furthermore, we proposed a novel method to characterize the comprehensive formation FNXS by weighting the FNXS responses of the major constituent minerals. Simulation results

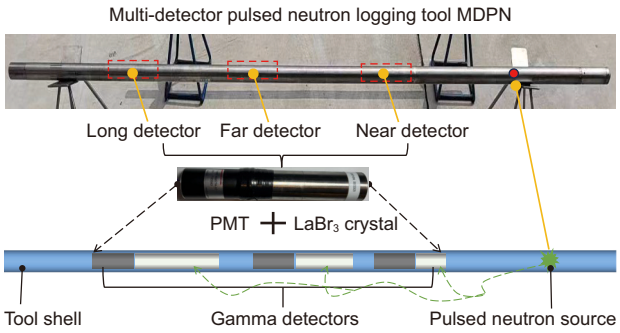

Fig. 5. The schematic diagram of the pulsed neutron saturation logging tool and formation model.

confirm the validity of this method and demonstrate its capability for more accurate gas zone delineation.

3.1. Construction of numerical model

As depicted in Fig. 5, the simulation model employs a freshwater-filled borehole with a 21.59 cm caliber, surrounded by a formation where porosity is adjusted between 0% and 20%. High-energy fast neutrons (14.1 MeV) are generated by a bottom-mounted D–T source and radiated uniformly into the surrounding rock. The detection system comprises three $LaBr_3$ scintillators located at source-to-detector distances of 35.8, 54.7, and 81.4 cm. These crystals have identical diameters (2.4 cm) but varying lengths of 5.08, 10.16, and 15.23 cm.

To ensure statistical precision, a total of 300 million particles were tracked in the simulation. The neutron generator operates with a 30 μs pulse width within a 160 μs repetition cycle, releasing 14.1 MeV high-energy neutrons. This sequence repeats for 30 cycles. For data acquisition, the detectors capture inelastic gamma-ray spectra during the 26–56 μs gate and capture gamma-ray spectra in the subsequent 62–160 μs window.

Monte Carlo numerical simulation was employed to construct the required models based on the mineral composition of matrix in the buried hill reservoirs. The wellbore diameter is set to 21.59 cm, with the wellbore filled with pure water. The formation matrix minerals and fluids are assumed to be uniformly distributed within the formation.

Firstly, six sets of models were established with quartz, calcite, dolomite, K_feldspar, Na_feldspar, and biotite individually serving as the matrix of the formation. For each model, formation porosities were set to 1%, 5%, 10%, 15%, and 20%, respectively. The pore space was entirely filled with either gas or fresh water. By collecting the inelastic gamma counts from the long detector, the FNXS response patterns to gas- and water-filled formation were obtained for different matrix minerals. To avoid restricting the applicability of the method solely to low-porosity buried hill formation, the model set also includes the porosity case of 20%. This allows the FNXS–based approach to remain valid for reservoirs where lithological complexity exists without significant porosity reduction.

Additionally, six complex mineral formation models were constructed based on mineral compositions derived from experimental analysis, such as core sampling and thin–section identification, to represent possible lithologies in the formation. These mineral compositions were chosen to reflect realistic formation conditions, with each set of models designed to simulate a range of lithological scenarios typically encountered in the Bohai Sea buried hill reservoirs. The mineral composition of different models is shown in Table 1. Among them, four sets are carbonate rock formation models, and two sets are granite gneiss formation models. The formation porosity is set to 10%, with the pores composed of gas and fresh water. The gas saturation is set to 0%, 20%, 40%, 60%, 80%, and 100%. The logging responses of the tool were simulated under different formation environments, and the inelastic gamma counts and capture gamma counts from each detector were collected.

3.2. Construction of the FNXS inversion model database for key minerals

The calculation of lithology weighting $FNXS_{lith}$ requires the prior construction of an FNXS inversion model database for the key minerals present in the formation. This model database facilitates the weighted calculation of FNXS in actual wells based on the key minerals compositions provided by lithology profiles.

Section 3.1 simulates the logging responses of six key minerals commonly found in buried hill formation, each individually serving as the matrix under gas-saturated and water-saturated conditions. The relationship between the logarithm of the inelastic gamma counts (LGRAT) from the long detector and the integrated formation FNXS for each model is shown in Fig. 6.

Based on the response characteristics of key minerals, an FNXS modeling database for dominant minerals in buried hill reservoirs can be established. Eqs. (9)–(14) represent the FNXS inversion models for calcite, dolomite, quartz, K_feldspar, Na_feldspar, and biotite, respectively. Red is uniformly used to represent gas–filled conditions, and blue is used to represent water–filled conditions. Different marker shapes and line styles are applied to distinguish the various matrix minerals.

$$FNXS_{calcite} = -3.06LGRAT + 24.282 \quad (9)$$

$$FNXS_{dolomite} = -3.32LGRAT + 25.447 \quad (10)$$

$$FNXS_{quartz} = -3.88LGRAT + 29.093 \quad (11)$$

$$FNXS_{K\_feldspar} = -2.895LGRAT + 25.733 \quad (12)$$

$$FNXS_{Na\_feldspar} = -3.114LGRAT + 27.614 \quad (13)$$

Table 1
Mineral composition and content of formation models.

Model	Calcite, %	Dolomite, %	Quartz, %	K_feldspar, %	Na_feldspar, %	Biotite, %	Chlorite, %	Illite, %	Kaolinite, %
1	0.10	0.80	0.05	0	0	0	0.01	0.03	0.01
2	0.15	0.75	0.02	0	0	0	0.02	0.04	0.02
3	0.45	0.50	0.01	0	0	0	0.01	0.02	0.01
4	0.55	0.35	0.02	0	0	0	0.02	0.05	0.01
5	0.05	0	0.41	0.34	0.34	0.08	0.01	0.06	0.01
6	0.01	0	0.18	0.44	0.44	0.14	0.02	0.10	0.02

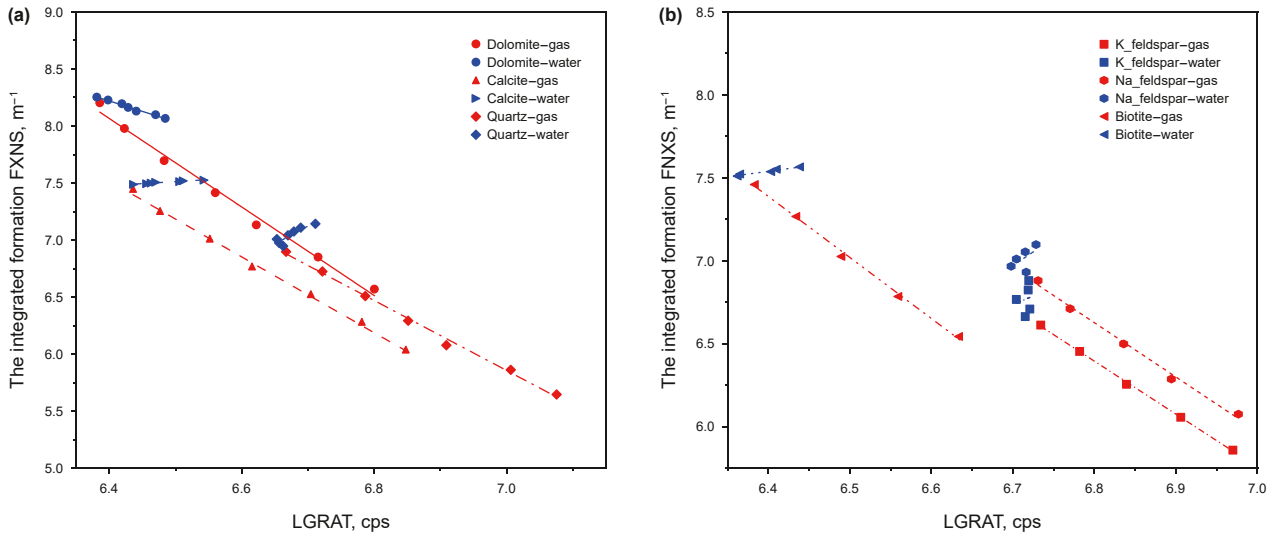

Fig. 6. FNXS response characteristics of key minerals. **(a)** Common minerals; **(b)** main minerals in granite gneiss.

$$FNXS_{biotite} = -3.499LGRAT + 29.557 \quad (14)$$

Meanwhile, according to the response characteristics, it is evident that the FNXS variation caused by the rock matrix is significant, indicating the necessity of conducting dynamic gas reservoirs evaluation.

3.3. Method validation in complex reservoirs

Based on the FNXS model database of key minerals constructed in Section 3.2, the integrated formation FNXS values ($FNXS_{lith}$) under the six sets of complex model conditions defined in Section 3.1 were calculated using the lithology weighting method in Eq. (5). Simultaneously, the corresponding integrated formation FNXS values were also calculated using the conventional method for comparison with the new method.

As shown in Fig. 7, the $FNXS_{lith}$ calculated by the proposed method deviates from the true model-defined FNXS by less than 1%. In contrast, as illustrated in Fig. 8, the FNXS derived from conventional methods exhibits an error of up to 6% in complex reservoirs.

After obtaining the accurate integrated formation FNXS, it is necessary to calculate the dynamic reference value for gas reservoirs evaluation–$FNXS^{w}_{sum}$.

According to Eq. (7), the FNXS values for the formation matrix under different mineral models set in the first section are obtained, as shown in Table 2.

The gas reservoirs reference values ($FNXS^{w}_{sum}$) under different models were calculated using the matrix FNXS, and the δ_d was computed using Eq. (8). As shown in Fig. 9, for each model with a different gas saturation, the $FNXS_{lith}$ is lower than $FNXS^{w}_{sum}$, resulting in $\delta_d > 0$, which effectively indicates the presence of gas reservoirs. For gas saturations of 40% and above–representing realistic reservoir conditions–the relative difference between $FNXS_{lith}$ and $FNXS^{w}_{sum}$ exceeds 2.8% for all six models, which is sufficiently large to ensure reliable gas reservoirs discrimination.

4. Application and analysis of the case study

To validate the practical application of the proposed gas reservoirs identification methodology, processing and analysis of actual well were conducted.

4.1. Calibration of XRF data

In practical applications of $FNXS^{w}_{sum}$ for dynamic gas reservoirs identification, XRF data need to be incorporated. Therefore, calibration of the XRF data is performed firstly.

To verify the accuracy of the lithology profile derived from XRF correction, wells X and Y within the Bohai Sea buried hill structure were selected as case studies. This research analyzed 32 core samples from the target zone, where the lithology is dominated by Archean granite gneiss and Paleozoic carbonates. The mineral assemblage primarily includes quartz, K-feldspar, albite, dolomite, and calcite, along with clay minerals such as biotite, illite, chlorite, and kaolinite.

Based on the major rock-forming minerals and their respective contents provided by the lithology profile corrected using XRF logging data, we calculated the matrix FNXS using Eq. (7). These calculated results were then benchmarked against the matrix FNXS values derived from mineral compositions determined by X-ray diffraction (XRD). The cross-validation, as depicted in Fig. 10,

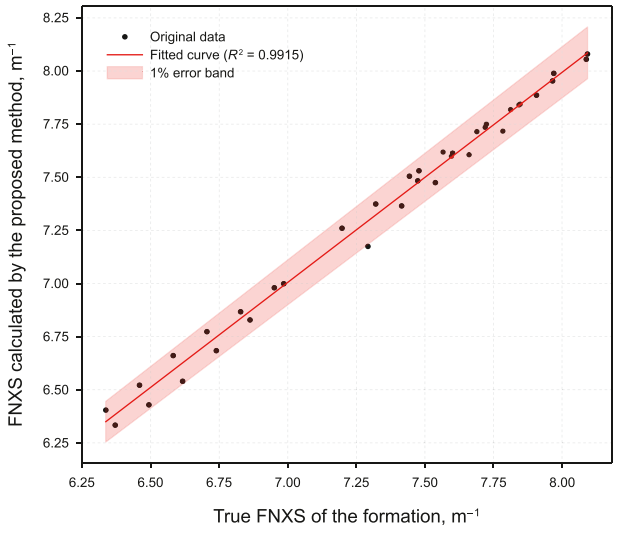

Fig. 7. FNXS calculated by the proposed method.

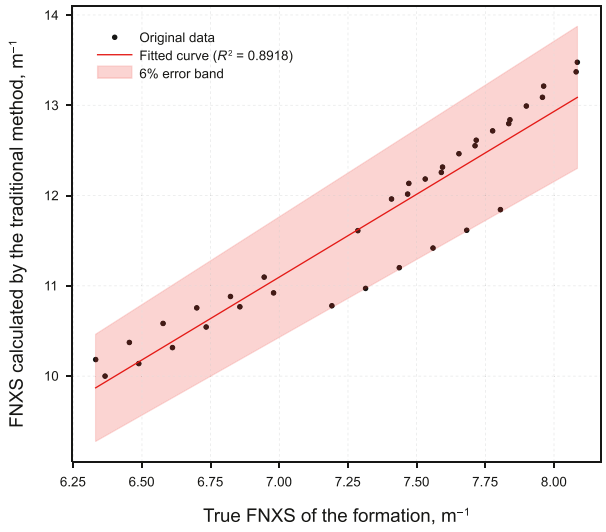

Fig. 8. FNXS calculated by the traditional method.

Table 2
Formation matrix FNXS values under different mineral model conditions.

Matrix FNXS, m^{-1}	Model 1	Model 2	Model 3	Model 4	Model 5	Model 6
$FNXS_{matrix}$	8.08	8.06	7.88	7.75	6.86	6.84

demonstrates a strong consistency between the two datasets. With an average relative deviation not exceeding 1.5%, the method proves to be highly reliable for practical deployment in the field.

4.2. Calibration of the FNXS model library for field application

To accurately apply the Monte Carlo–based FNXS model library to field measurements, a calibration procedure was required to reconcile simulated and measured count rates. It is important to note that the calibration was not performed by pairing each simulated point with a corresponding measurement from the same well. Instead, both simulated and measured data were independently correlated with formation density, and density served as a physical intermediary to establish the conversion between simulated and measured count rates.

As illustrated in Figs. 11 and 12, several limestone calibration wells were selected, and their pure inelastic gamma count rates were extracted and regressed against density. In parallel, Monte Carlo models were constructed to reproduce the measurement conditions of the calibration wells, from which simulated pure inelastic gamma count rates were also regressed against density. Because both simulated and measured responses exhibit a stable and monotonic dependence on density for a single lithology, the two regression relationships can be combined to derive a gain–shift conversion function that maps simulated count rates to their measured equivalents. This density-based indirect calibration avoids the need for one-to-one matching between simulated and measured points at the same wells, and therefore extends the applicability of the conversion to arbitrary porosity and measurement environments.

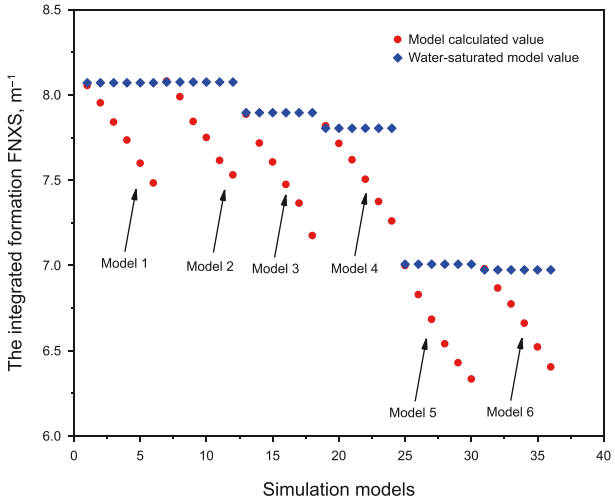

Fig. 9. Dynamic gas reservoirs identification of the six models.

By comparing simulated and measured responses, a calibration formula (Eq. (15)) was obtained, which enables the logarithm of the simulated long detector inelastic gamma count rate to be converted into the logarithm of the measured count rate. This conversion allows the FNXS model library to be used directly with actual logging data.

$$LGRAT1 = 1.227 \cdot LGRAT2 + 22.88 \quad (15)$$

LGRAT1 represents the logarithm of the measured long detector inelastic gamma count rate, and LGRAT2 represents the logarithm of the simulated long detector inelastic gamma count rate. Using the above conversion relationship, the simulated FNXS model library can be transformed into a form consistent with field logging responses, enabling its application to real–well interpretation.

4.3. Processing results of well X

Situated within a buried hill complex, Well X benefits from two adjacent hydrocarbon-rich sags and a pervasive fracture network that serves as an effective migration conduit. These factors establish a high potential for reservoirs accumulation (Tan et al., 2015). The well was subjected to standard logging procedures—such as resistivity, acoustic, imaging, and neutron-density surveys—prior to the pulsed neutron operation. Petrophysical evaluation of the openhole logs indicates an average porosity of 8% and low water salinity. The rock matrix is primarily composed of limestone and dolomite intercalated with granite gneiss, with illite

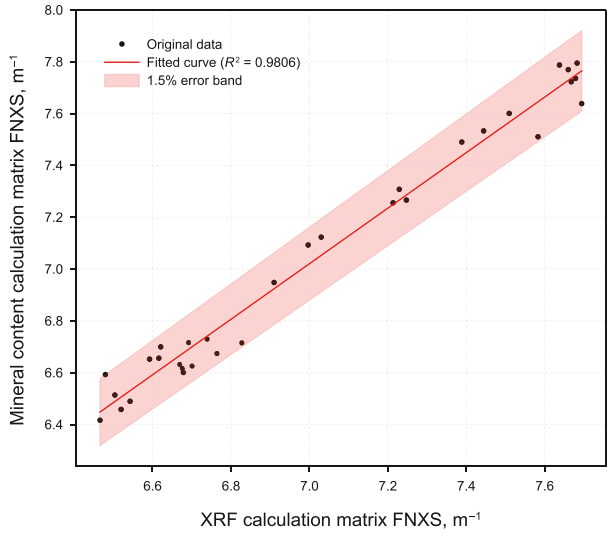

Fig. 10. Comparison between matrix FNXS calculated from elemental content and theoretical values.

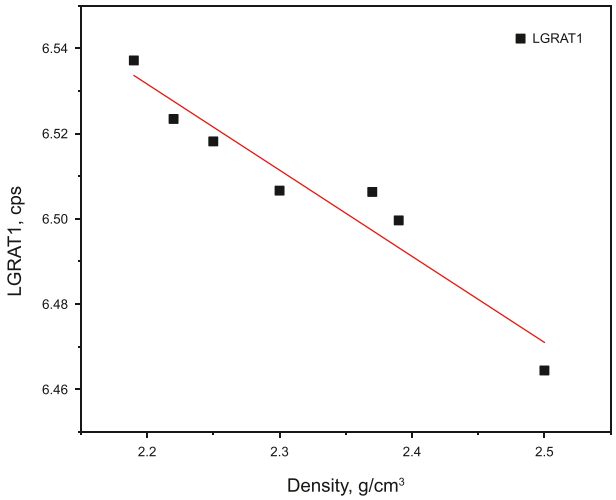

Fig. 11. Response of simulated long detector inelastic gamma count rate as a function of formation density.

being the major clay mineral alongside minor chlorite and kaolinite.

$FNXS_{lith}$ and the matrix FNXS are calculated by weighting based on the lithology profile and XRF information. Then, combined with the effective porosity curve, the FNXS of the water–saturated formation pores is obtained by weighting the matrix FNXS and the FNXS of pure water.

The suite of logging curves is presented in Fig. 13, which is partitioned into six tracks: track 1 displays the Stoneley wave amplitude curves; track 2 includes the porosity and density curves; track 3 shows the effective porosity curve; track 4 shows the gas reservoirs identification based on FNXS calculated using the traditional method; track 5 displays the FNXS curves, where $FNXS_{lith}$ represents the comprehensive formation FNXS curve and $FNXS_W$ denotes water-saturated formation FNXS curve; track 6 presents the gas detection curve.

Three distinct gas reservoirs intervals—X830–X855 m (Fig. 13(a)), X857–X865 m (Fig. 13 (b)), and X867–X890 m (Fig. 13 (c))—were identified through the integrated analysis of FNXS and detector responses. The gas reservoirs nature of these zones is primarily substantiated by the $FNXS_{lith}$ curve falling markedly below the $FNXS^{W}_{sum}$ baseline, an observation that aligns with the low hydrogen index inferred from the separation between long- and near-spaced gamma count rates. Regarding reservoirs effectiveness, the suppressed GR values in these layers, combined with the presence of conductive and effective fractures identified via electrical and acoustic imaging, indicate high-quality reservoirs conditions. This interpretation is further corroborated by the overall low values of the Stoneley wave amplitude curve, which exhibits significant sectoral variations (particularly within X867–X880 m) and the notable methane fluctuations recorded in the gas logs.

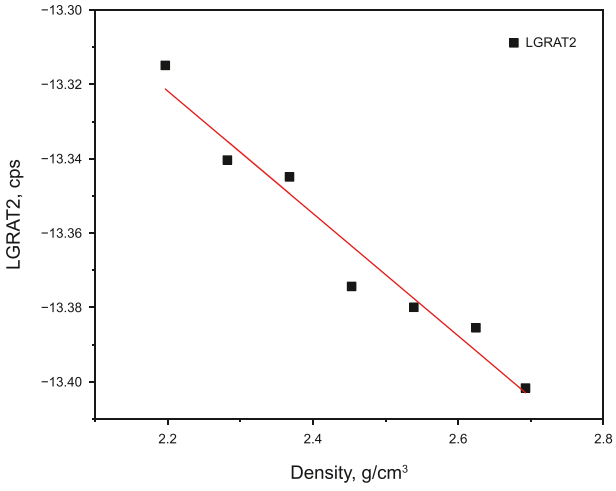

Fig. 12. Response of measured long detector inelastic gamma count rate from calibration wells as a function of formation density.

Additionally, the drill stem test (DST) results conducted for these intervals yielded a gas production rate of 223417 m^3/d. These observations collectively validate the effectiveness of the proposed gas evaluation method.

To quantitatively evaluate the effectiveness of the proposed method, the sensitivity of gas–reservoir identification was compared between the traditional method and the method proposed in this study. To eliminate the influence of curve amplitude on sensitivity assessment, the FNXS curves obtained by the traditional method and the proposed method were first normalized. This prevents the comparison from being dominated by amplitude differences and better reflects the true reliability of gas indications. The sensitivity of both methods was then calculated using Eq. (16).

$$S = \frac{\left|FNXS_{norm} - FNXS_{refnorm}\right|}{FNXS_{refnorm}} \cdot 100\% \quad (16)$$

where $FNXS_{norm}$ and $FNXS_{refnorm}$ represent the normalized FNXS curve and the normalized gas–reference value, respectively.

The calculated results show that the average sensitivity of the traditional method is 30%, while that of the proposed method reaches 62%, indicating an approximate two-fold enhancement. Moreover, the proposed method identifies three gas–reservoir intervals with a cumulative reservoir thickness of 56 m in this well, compared with four intervals totaling 64 m interpreted by the traditional approach. Overall, the proposed method attains a gas-layer thickness match rate of 87.5%.

4.4. Processing results of well Y

The Y well is located in a strike-slip overlap zone, characterized by well-developed fractures, favorable reservoir quality, and superior hydrocarbon accumulation conditions. Conventional logging data indicate that the primary lithologies in this well are tuff, rhyolite, and andesite, with predominant mineral compositions including quartz, potassium feldspar, sodium feldspar, biotite, illite, kaolinite, and chlorite. The lithology is complex, making evaluation challenging.

By integrating XRF logging data with lithological profile information, the $FNXS_{lith}$ and $FNXS^{W}_{sum}$. As illustrated in Fig. 14, the logging curves are arranged as follows: track 1 displays the natural gamma ray (GR) and borehole diameter curves; track 2 displays the resistivity curve; track 3 contains the porosity and density curves; track 4 presents the effective porosity curve; track 5 shows the gas reservoirs identification based on FNXS calculated using the traditional method; track 6 displays the FNXS calculated using the proposed method; track 7 presents the gas detection curve; track 8 illustrates the lithology profile.

In the depth interval of X865–X874 m (Fig. 14(a)), the gas detection curve exhibits a significant increase, with a high GR reading and a notable decrease in resistivity. The deep resistivity measurement is 18.1 Ω m. The neutron–density crossover is

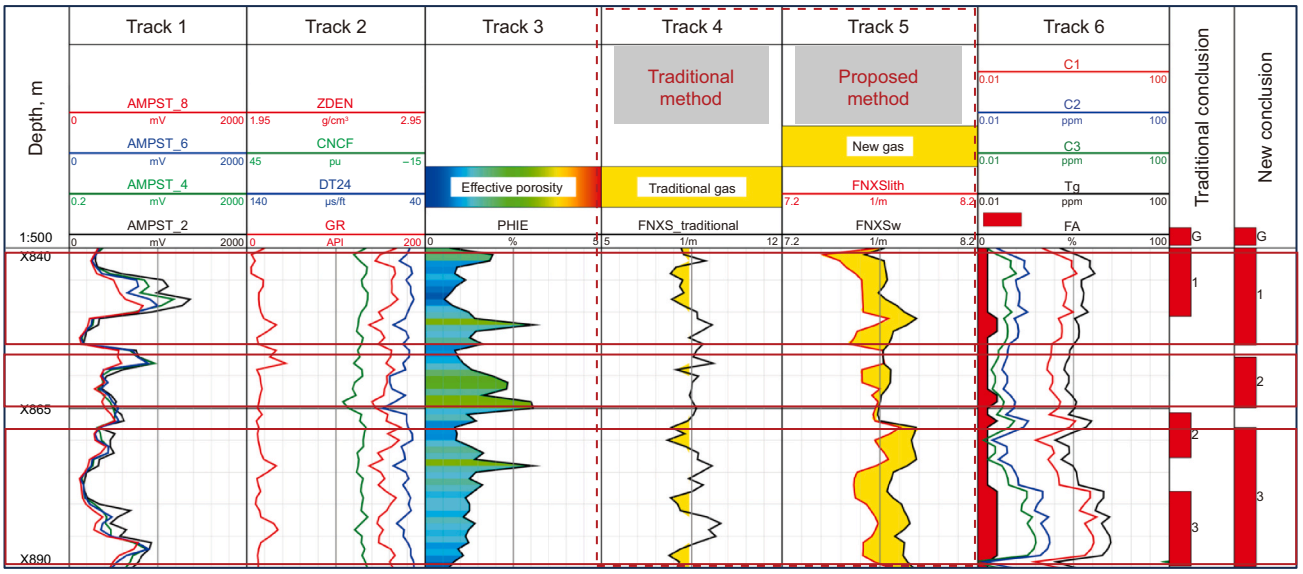

Fig. 13. Interpretation case of well X.

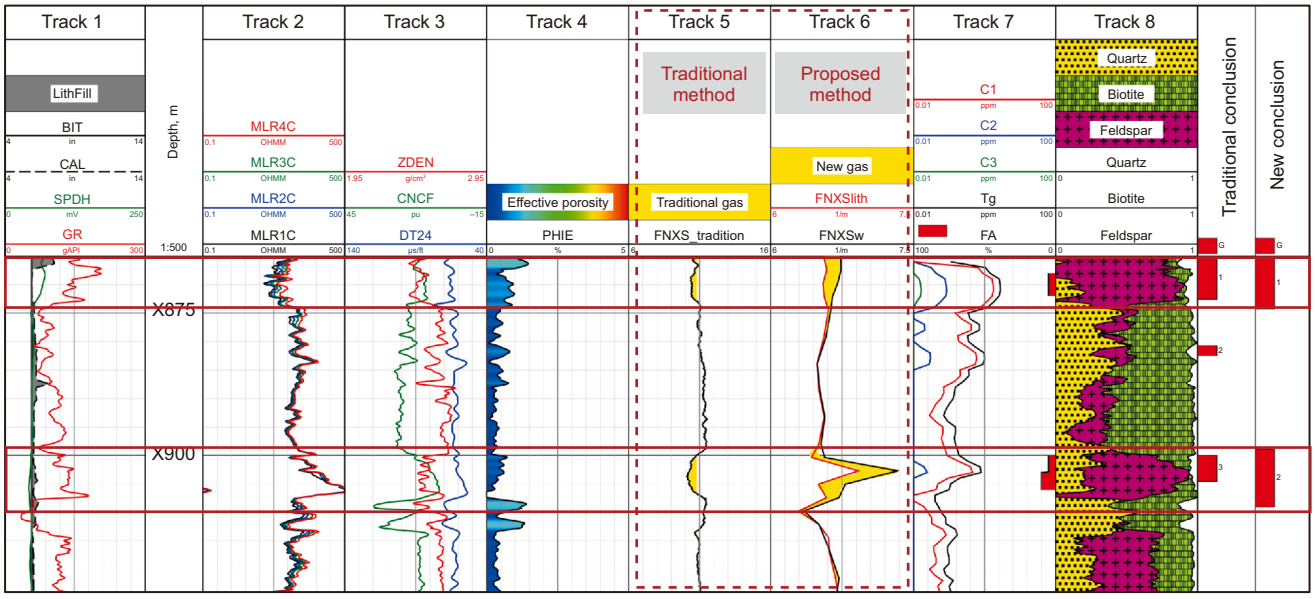

Fig. 14. Interpretation case of well Y.

evident, yielding a calculated porosity of 6.8% and a permeability of 23.6 mD.

In the X900–X908 m (Fig. 14(b)) interval, the GR readings remain high, while resistivity does not show a significant decline but exhibits slight differentiation. The deep resistivity measurement is 118.8 Ω m, and the acoustic travel time does not increase significantly. However, the gas detection curve displays a marked increase, and the neutron–density crossover is observed, with a calculated average porosity of 5.7%.

Across these two intervals, the gamma–ray count rate curves at different source distances exhibit distinct envelopment, and The $FNXS_{lith}$ curve is significantly lower than the $FNXS^{w}_{sum}$ curve. Based on these observations, the intervals are comprehensively evaluated as gas reservoirs. Meanwhile, the fluorescence test conducted on sidewall core samples from these intervals exhibited a blue response, which to some extent supports the validity of the interpretation.

Similarly, using Eq. (16), the gas reservoirs identification sensitivity in this well is calculated to be 24% for the traditional method and 52% for the method proposed in this study, representing approximately a two-fold improvement. The gas reservoirs thickness match rate obtained by the proposed method reaches 75%.

5. Discussion

The applicability of the proposed FNXS–based gas reservoirs identification method depends primarily on the accuracy of the lithology profile. Since the lithology weighting in this study is

performed using only the dominant matrix minerals, the calculated $FNXS_{lith}$ is sensitive to errors in mineral composition. Therefore, when the lithology profile is well constrained, the method is able to provide reliable gas–reservoirs identification in complex buried hill reservoirs.

However, a key limitation of the current workflow is its dependence on XRF logging data to correct the lithology profile. The accuracy of the method increases significantly when the XRF–derived elemental abundances are used to constrain mineral content before performing lithology weighting and dynamic gas identification. If XRF logging is not available, the FNXS curve obtained from lithology weighting alone can still be used to rapidly screen potential gas reservoirs intervals, but the accuracy of gas reservoirs identification is reduced. To achieve high–precision interpretation, lithology calibration using XRF data remains necessary.

6. Conclusion

This paper focuses on gas reservoirs identification in the Bohai Sea buried hill reservoirs. To overcome the influence of complex lithology, the conventional FNXS calculation method was improved to obtain accurate formation FNXS values, and a dynamic gas reservoirs reference value was constructed and applied to gas reservoirs identification in the complex buried hill reservoirs of the Bohai Sea. The study provides an effective method for gas reservoirs evaluation under complex lithological conditions. The specific conclusions are as follows:

(1) To overcome the influence of lithology, a lithology weighting FNXS calculation method were theoretically derived. The FNXS obtained by performing weighted fitting of the single–mineral FNXS inversion formulas using the key minerals contents provided by the XRF–calibrated lithology profile achieves higher accuracy. Meanwhile, to address the challenge of gas reservoirs classification caused by variations in matrix FNXS, the use of $FNXS^{w}_{sum}$ as a dynamic reference value for gas reservoirs identification is proposed.
(2) Six sets of complex formation models were established and numerically simulated using Geant4 to validate the proposed method. The $FNXS_{lith}$ calculated by the new approach shows an error of less than 1% compared to the theoretical values. The dynamic gas reservoirs reference value $FNXS^{w}_{sum}$ also provides high accuracy in gas reservoirs identification under complex reservoirs conditions.
(3) The proposed method was applied to a case well in the Bohai Sea buried hill reservoirs. The $FNXS_{lith}$ curve, calculated based on XRF data and lithology profiles, demonstrated significantly higher sensitivity and accuracy in gas reservoirs identification, with the sensitivity improved by approximately a factor of two compared with the traditional method. The interpretation results are consistent with DST results and mud gas logging data, verifying the effectiveness of the method.

CRediT authorship contribution statement

Zhen-Yang Li: Writing – original draft, Methodology, Conceptualization. **Jie Shang:** Supervision, Resources, Project administration, Funding acquisition, Conceptualization. **Jia-Wei Zhang:** Resources, Project administration. **Qiong Zhang:** Writing – review & editing, Project administration, Data curation. **Quan-Ying Zhang:** Writing – review & editing, Investigation.

Declaration of competing interest

The authors declare that they have no known competing financial interests or personal relationships that could have appeared to influence the work reported in this paper.

Acknowledgements

The authors acknowledge the China Natural Science Fund (Grant No. U23B20151) for support.

References

Al-Qasim, A., Mostefai, I., Kokal, S., et al., 2019. Formation evaluation using advanced pulsed neutron tools. In: SPE Gas & Oil Technology Showcase and Conference, SPE–198541–MS. https://doi.org/10.2118/198541-MS.
Badruzzaman, A., Logan, J., Bean, C., et al., 2007. Is accurate gas/steam determination behind pipe feasible with pulsed neutron measurements?. In: Asia Pacific Oil and Gas Conference and Exhibition, SPWLA–110098–MS https://doi.org/10.2118/110098-MS.
Carpenter, C., 2018. Pulsed-neutron comparison of open- and casedhole wells: An Alaskan case study. J. Petrol. Technol. 70 (8), 54–56. https://doi.org/10.2118/0818-0054-JPT.
Chadwick, M.B., Obložinský, P., Herman, M., et al., 2006. ENDF/B–VII.0: Next generation evaluated nuclear data library for nuclear science and technology. Nucl. Data Sheets 107 (12), 2931–3060. https://doi.org/10.1016/j.nds.2006.11.001.
Fan, J-L, Zhang, Q, Jin, Y, et al., 2024. Evaluation of cement density utilizing through-casing X-Ray logging method. Petrol. Sci. 22 (3), 1041–1050. https://doi.org/10.1016/j.petsci.2024.11.004.
Guo, P., Fitz, D., Spears, R., 2010a. Pulsed neutron logging in tight gas sand reservoirs: A cost effective evaluation approach. In: SPWLA 51th Annual Logging Symposium, SPWLA–2010–21847.
Guo, W., Jacobson, L., Truax, J., et al., 2010b. A new three-detector 1-11/16-inch pulsed neutron tool for unconventional reservoirs. In: SPWLA 51th Annual Logging Symposium, SPWLA–2010–48800.
Hou, M.C., Cao, H.Y., Li, H.Y., et al., 2019. Characteristics and controlling factors of deep buried-hill reservoirs in the BZ19-6 structural belt, Bohai sea area. Nat. Gas. Ind. B. 6, 305–316. https://doi.org/10.1016/j.ngib.2019.01.011.
Hu, Z., Xu, C., Yang, B., et al., 2017. Reservoir forming mechanism of Penglai 9-1 granite buried-hills and its oil geology significance in Bohai Sea. Shiyou Xuebao/Acta Petrolei Sinica 38, 274–285. https://doi.org/10.7623/syxb201703004 (in Chinese).
Kim, Y., Boyle, K., Chace, D., et al., 2017. Innovative triangulation technique enables simultaneous determination of three-phase formation fluid saturations using pulsed neutron logging. In: SPWLA 58th Annual Logging Symposium. SPWLA–2017–GG.
Kowalska, S., Kubik, B., Skupio, R., et al., 2020. Downhole lithological profile reconstruction based on chemical composition of core samples and drill cuttings measured with portable X-ray fluorescence spectrometer. Minerals 10 (12), 1101. https://doi.org/10.3390/min10121101.
Kwong, K., Liu, Z., Guo, W., et al., 2013. Case history: monitoring gas (CO_2) flood in a carbonate reservoir with a new slim multidetector pulsed neutron tool. In: SPE Enhanced Oil Recovery Conference, SPE–165230–MS. https://doi.org/10.2118/165230-MS.
Li, H.-G., Zhang, X.-G., Guo, H.-Z., et al., 2019. A new measurement of evaluating gas or CO_2 in formation - fast neutron cross section. In: SPWLA 25th Formation Evaluation Symposium of Japan, SPWLA–JFES–2019–G.
Li, H., Niu, C., Xu, P., et al., 2021. Discovery of bozhong 13-2 Archean large monoblock volatile buried hill oilfield and its oil and gas exploration significance. Nat. Gas. Ind. B 8 (4), 376–383. https://doi.org/10.1016/j.ngib.2021.07.008.
Li, Z., Zhang, Q., Li, J., et al., 2025. A method on the application of pulsed neutron logging for gas reservoirs identification of the buried-hill in Bohai Sea. In: SPWLA 66th Annual Logging Symposium, SPWLA–2025–0055. https://doi.org/10.30632/SPWLA-2025-0055.
Liu, J., Liu, S., Zhang, F., et al., 2018. A method for evaluating gas saturation with pulsed neutron logging in cased holes. J. Nat. Gas Sci. Eng. 59, 354–362. https://doi.org/10.1016/j.jngse.2018.09.018.
Rose, D., Zhou, T., Saldungaray, P., 2017. Solving for reservoir saturations using multiple formation property measurements from a single pulsed neutron logging tool. In: SPWLA 58th Annual Logging Symposium, SPWLA–2017–II.
Tan, Z., Lu, X., Zhao, T., 2015. Tectonic characteristics and its effects on the control of the oil and gas accumulation in bayanhushu depression. In: The 2015 2nd International Conference on Engineering Technology and Application, vol. 22, 04025. https://doi.org/10.1051/matecconf/20152204025.
Trcka, D., Gilchrist, A., Riley, S., et al., 2006. Field trials of a new method for the measurement of formation gas using pulsed-neutron instrumentation. In: SPE Annual Technical Conference and Exhibition, SPE–102350–MS. https://doi.org/10.2118/102350-MS.
Velker, N.N., Banzarov, B.V., Inanc, F., et al., 2012. Geant4 for solving nuclear geophysics problems. In: SPE Russian Oil and Gas Exploration and Production

Technical Conference and Exhibition, SPE-162008-MS. https://doi.org/10.2118/162008-MS.
Wang, D., Wang, Q., Liu, X., et al., 2019. Characteristics and developing patterns of gneiss buried hill weathering crust reservoir in the sea area of the Bohai Bay Basin. Acta Petrol. Sin. 35 (4), 1181–1193. https://doi.org/10.18654/1000-0569/2019.04.13 (in Chinese).
Zett, A., Webster, M., Spain, D., et al., 2012. Application of new generation multi detector pulsed neutron technology in petrophysical surveillance. In: SPWLA 53th Annual Logging Symposium, SPWLA–2012–094.
Zhou, T., Rose, D., Quinlan, T., et al., 2016. Fast neutron cross-section measurement physics and applications. In: SPWLA 57th Annual Logging Symposium, SPWLA–2016–EE.